Journal of Extracellular Biology

SHORT COMMUNICATION OPEN ACCESS

Cell Envelope Remodeling and Lipid Metabolism Coordinate Extracellular Vesicle Output in Mycobacterium Tuberculosis

José L. Serrano-Mestre[1] | Laura Lerma[1] | Lucía Vázquez-Iniesta[1] | Vivian C. Salgueiro-Toledo[1] | Ainhoa Palacios[2] | Sogol Alebouyeh[1] | Andrea Doddi[3] | Felix Elortza[2] | Mikel Azkargorta[2] | Leticia Sampedro[2] | Estibaliz Atondo[2] | Miguel Ángel Pacual-Itoiz[2] | Oren Mayer[4] | Torin Westwood[5] | William R. Jacobs Jr[5] | Rafael Prados-Rosales[1]

[1]Department of Preventive Medicine and Public Health and Microbiology, Autonoma University of Madrid, Madrid, Spain | [2]CIBERehd, CICbioGUNE, Basque Research and Technology Alliance (BRTA), Derio, Bizkaia, Spain | [3]Department of Genetics, Campus de Excelencia Internacional Agroalimentario ceiA3, Universidad de Córdoba, Córdoba, Spain | [4]Centers for Disease Control and Prevention, Atlanta, Georgia, USA | [5]Department of Microbiology and Immunology, Albert Einstein College of Medicine, Bronx, New York, USA

Correspondence: Rafael Prados-Rosales (rafael.prados@uam.es)

Received: 23 January 2026 | **Revised:** 13 May 2026 | **Accepted:** 24 May 2026

Keywords: extracellular vesicles | mycobacterium tuberculosis | screening | transposon mutants

ABSTRACT

Tuberculosis (TB), caused by *Mycobacterium tuberculosis* (*Mtb*), remains a leading global cause of death due to the pathogen's highly adaptive physiology and its ability to manipulate host immunity. Despite extensive study, our understanding of *Mtb* biology during infection remains incomplete, limiting the development of new diagnostics, therapeutic and vaccine strategies. The *Mtb* cell envelope and its associated secretion systems are central to virulence and immune evasion. *Mtb* releases extracellular vesicles (EVs) that carry immunomodulatory molecules, including lipoproteins, which influence immune responses. Although individual genes and environmental cues have been shown to alter vesiculogenesis, a genome-wide dissection of EV biogenesis has not been attempted. Here, we establish a high-throughput screening system to identify *Mtb* mutants with altered EV production using a 96-well filtration platform combined with a lipophilic dye or an *Mtb*-EV (MEV)-specific antibody. Our genome-wide screen revealed genes in cell envelope remodeling and fatty acid metabolism are major regulators of vesiculogenesis. These findings provide a robust platform for defining the molecular determinants of MEV production and lay the groundwork for mechanistic characterization of vesicle biogenesis in *Mtb*.

1 | Introduction

One of the many reasons why we have not generated all the necessary tools against TB is the incomplete knowledge of *Mtb*´s physiology, which happens to be very difficult to study during human infection. It is widely accepted that *Mtb* has generated exquisite mechanisms of immunomodulation and immune evasion, many of which depend on its cell envelope (Dulberger et al. 2019) and its capacity to secrete/release bacterial factors (Abdallah et al. 2007). Mycobacteria, along with practically all forms of life, can also export biomolecules, such as proteins, lipids, glycolipids or nucleic acids packed within extracellular vesicles (EVs) (Prados-Rosales et al. 2011; Brown et al. 2015). Since the first detection of bacterial EVs more than 60 years ago in

José L. Serrano-Mestre and Laura Lerma authors contributed equally to this work.

Escherichia coli (Bishop and Work 1965), subsequent studies have demonstrated their functional commonality despite differences in bacterial cell envelope architecture. Bacterial EVs are "spherical, membranous vesicles from microbial cell surfaces ranging in size from 20 to 500 nm in diameter" (Brown et al. 2015; Schwechheimer and Kuehn 2015). *Mtb* produces EVs in vitro and in vivo as part of a sophisticated mechanism to manipulate host cellular physiology and evade the host immune system (Prados-Rosales et al. 2011; Athman et al. 2015). EVs from pathogenic mycobacterial strains are enriched in lipoproteins, which are well-known immunomodulatory molecules, and induce a TLR-2-dependent inflammatory response in vitro and in vivo (Prados-Rosales et al. 2011). Therefore, *Mtb* EVs (MEVs) production may provide an alternative mechanism for transport of immunomodulatory compounds such as lipoproteins, leading to the distribution of these compounds to various compartments within infected host cells or to exosomes. Thus, the generation and release of MEVs may allow mycobacteria confined within phagosomes to deliver virulence factors to other cellular compartments and/or into the extracellular milieu to affect the physiology of neighboring cells. Moreover, MEVs have strong immunogenicity in vitro and when administered to mice (Prados-Rosales et al. 2011; Prados-Rosales et al. 2014), possess promising vaccine properties (Prados-Rosales et al. 2014), and are source of biomarkers for TB (Ziegenbalg et al. 2013; Schirmer et al. 2022). Consequently, MEVs have generated considerable interest for their potential role in TB pathogenesis and their implications in development of new preventive and therapeutic antitubercular strategies.

The biogenesis of bacterial EVs strongly depends on the architecture of the cell envelope. Thus, gram negative bacteria have two main routes of vesicle formation. Outer membrane vesicles (OMVs) can be produced via blebbing of the outer membrane (OM). These OMVs encapsulate components from the periplasmic space before detaching and release to the extracellular space. Alternatively, Gram negative bacteria can generate EVs through a process termed explosive cell lysis, generating outer-inner membrane vesicles (Schwechheimer and Kuehn 2015; Toyofuku et al. 2019). In Gram-positive bacteria bubbling gives rise to cytoplasmic membrane vesicles (Toyofuku et al. 2019) as they lack OM. In *Streptococcus aureus* the generation of EVs is supported by peptides with surfactant activity and by autolysins hydrolyzing highly cross-linked PG (Wang et al. 2018). More recently, it was shown that a closely related species with *Mtb* such as *Corynebacterium glutamicum* can produce EVs from both the cell membrane and the outer membrane (Nagakubo et al. 2021).

Considering the complexity of the vesiculogenesis process it is conceivable that multiple genes might control the production and release of a piece of cell membrane in the form of EV. In this context, there have been several attempts to genetically dissect the biogenesis of EVs in gram negative bacteria (Nevermann et al. 2019; McBroom et al. 2006). Both in *E.coli* and *Salmonella enterica* serovar Typhi (S. Typhi), gene disruptions that seem to affect outer membrane vesicle (OMV) production are related to lipoprotein Omp expression, peptidoglycan synthesis, LPS synthesis and the σE envelope stress response. Therefore, the genetics governing EV in gram negative bacteria is related to processes linked to the homeostasis of the cell envelope. The mycobacterial cell envelope is particularly complex compared to other bacterial species since PG is covalently linked to the polysaccharide arabinogalactan (AG), which in turn is decorated with exceptionally long-chain (up to 60 Cs) mycolic acids (MA) (Daffé 2015; Kalscheuer et al. 2019). Therefore, if MEV biogenesis and release follow similar routes as in gram negative bacteria a profound remodeling of the cell envelope is needed so that EVs can reach the extracellular space. Regarding genetics underlying the vesiculogenesis process in *Mtb*, it is known that MEV production is an active process regulated by iron (Prados-Rosales et al. 2014), the cell envelope related protein VirR (vesiculogenesis and immune response regulator) (Rath et al. 2013), the two-component system SenX3-RegX3 (White et al. 2018) and the bacterial dynamin-like proteins IniA and IniC (Gupta et al. 2023). While iron limitation, a stressful condition encountered in the host, activation of SenX3-RegX3 signaling and expression of *iniAC* induce vesiculation, VirR expression restricts vesicle release; deletion of *virR* leads to hypervesiculation. Importantly, no bacterial species has yielded a completely deficient mutant in EV release, suggesting that vesiculation may be essential and controlled by multiple overlapping pathways.

To broaden our understanding, we performed a genome-wide analysis of MEV production using a saturated transposon (*Tn*) library in the double auxotroph mc^{2}6230 (ΔRD1Δ*panCD*) (Sambandamurthy et al. 2006). Our findings highlight fatty acid metabolism as a major determinant of MEV regulation in *Mtb*.

2 | Results

Auxotrophic *Mtb* strain mc^{2}6230 has similar capacity to release MEVs as *Mtb* H37Rv. Extracellular vesicle (EV) production in mycobacteria is dependent on growth kinetics (Prados-Rosales et al. 2011). To assess the suitability of the auxotrophic *Mtb* strain ΔRD1Δ*panCD* (mc^{2}6230) as a model for EV studies we first studied the growth in minimal medium (MM) and found a minor delay in the growth of mc^{2}6230 relative to WT (Figure 1A). We isolated MEVs from MM cultures at mid logarithmic phase of both strains and determined the size distribution and concentration of MEVs by nanoparticle tracking analysis (NTA). After normalizing by colony forming units (CFUs) we found no significant differences (Figure 1B). Additional determination of MEV levels in culture by dot blot using a MEV-binding polyclonal antibody (Prados-Rosales et al. 2014 Oct) revealed no differences in MEV quantity between strains (Figure 1C). These results suggest that both strains release MEVs in similar quantities when growing in MM.

Residual differences in whole cell and MEV protein composition between the auxotrophic *Mtb* strain mc^{2}6230 and WT *Mtb*. One potential source of variation between mc^{2}6230 and the WT strain is the whole cell or MEV protein composition. This fact could limit the use of the auxotrophic strain as a model to study MEVs. Consequently, we performed label-free peptide mass spectrometry (LF-MS) of whole cell lysates (WCLs) and isolated MEVs from axenic cultures to examine for potential impact of the mutations of the auxotroph strain on protein composition relative to WT *Mtb* (**Figure 2**, Table S1). Upon Principal Coordinate Analysis (PCoA) analysis of the proteomic profiles based on Bray-Curtis dissimilarities (Figure 2A), we found that the first principal component (PC1, 56.5% of total variance), separated the samples by cell compartments (WCLs vs

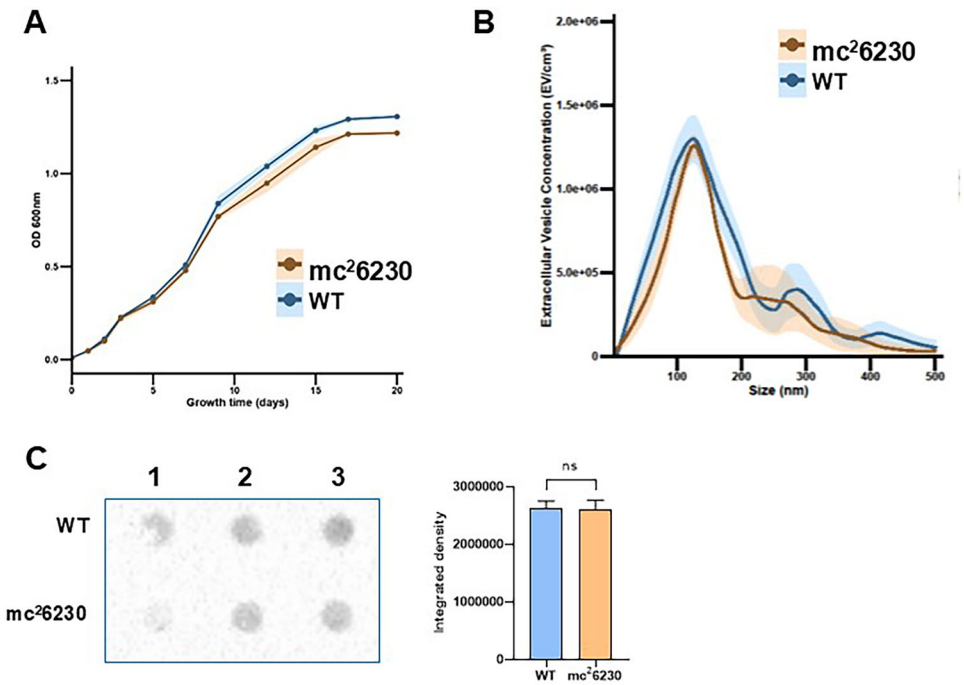

FIGURE 1 | Validation of the attenuated Mtb strain mc^{2}6230 as a model for extracellular vesicle (MEV) studies. (A) Growth kinetics of WT Mtb H37Rv and the auxotrophic strain mc^{2}6230 cultured in minimal medium. (B,C) Quantification of MEV release from WT and mc^{2}6230 by dot-blot (B) or NTA (C). Data are mean and standard of error from three biological replicates in B. Experiments were repeated twice with similar results. Size distribution curves represent averages from six biological replicates, demonstrating comparable particle size and abundance between strains.

EVs) regardless of the strain, while the second axis (PC2, 8.9% of total variance) captured the strain effects on the proteomic footprint only among EVs. Global statistical analysis confirmed that these grouping factors significantly drive the proteomic landscape (PERMANOVA: $R^2 = 0.695$, p-value = 0.001). These results suggest that differences in protein abundances between EVs and WCLs are larger than differences found between strains, and that, concerning the differences across strains, these are comparatively more important in EVs.

At whole cell level we detected 997 and 1090 proteins in lysates from WT and mc^{2}6230 strains, respectively. Proteomic data analysis found 19 significantly different proteins between both strains, 18 of them being more abundant in the auxotrophic strain. Notably, 15 out of these 18 proteins were exclusively detected in the lysate of the mc^{2}6230 strain (Figure 2B). The only differentially produced protein in the lysate of the WT strain was EspA (Rv3616c), an ESX-1 secreted antigen, which is absent in the RD1-deficient auxotrophic strain. The fact that less than 1% of the identified proteins are different between both strains explains why we could not find significant enrichments in biological processes after applying a gene ontology (GO) analysis.

Proteomic analysis of isolated MEVs showed a similar trend (Figure 2B). We could identify 979 and 965 proteins WT and mc^{2}6230 strains, respectively. Thirty-six proteins were statistically different between both MEVs and 14 of them were more abundant in MEVs from the auxotrophic strain, 5 of them being exclusive. The remaining 18 proteins were more abundant in WT MEVs, 9 of them as exclusive. As in the whole cell analysis, the GO analysis did not reveal any significant enrichment, suggesting that mutations in the auxotrophic strain do not impact the whole cell proteome nor the MEV cargo. These findings justify the use of the attenuated auxotroph mc^{2}6230 strain as model for dissecting MEV production.

The MEV screening system. MEVs are typically isolated from liquid culture using a protocol adapted from Gram-negative bacteria. MEVs are concentrated from a clarified supernatant prior to a density gradient ultracentrifugation (DGU) step, which allows separation of major mycobacterial cell surface-associated polysaccharides such as α-glucan from MEVs. A final step of dialysis prior to ultracentrifugation is needed to obtain a pure vesicle population (Prados-Rosales et al. 2011). This large-scale approach is not suitable to investigate vesiculogenesis in *Mtb* in a genome-wide manner. Consequently, we developed a high-throughput screening system to attempt the genetic dissection of MEV production. It captures and detects MEVs at submicrolitre level from *Mtb* liquid cultures using a series of stacked 384-well filtration plates. Detection of MEVs is accomplished using the FM4-64 lipophilic probe (McBroom et al. 2006)(1st screening) or with a MEV-specific antiserum in a dot-blot format (2nd screening) (Prados-Rosales et al. 2014; Gupta et al. 2023) (Figure 3A). We assessed the analytical performance of the system determining the limit of detection (LOD) and linearity range (LR) using FM4-64 (Figure 3B). Our system can detect up to 10^5 particles per ml and in a range between 10^5 and 10^9 EVs ml^{-1}. Validation of the screening system included testing the previously known genetic defects or environmental conditions that modulate vesiculation in *Mtb*. Specifically, we successfully confirmed the vesiculation phenotype of some hyper- and hypovesiculating mutants like *virR*^{mut} or Δ*iniA*, respectively (Figure 3C), as well as the impact on vesiculation of some growing conditions, like iron starvation or antibiotic exposure (Figure 3C) (Prados-Rosales et al. 2014; Gupta

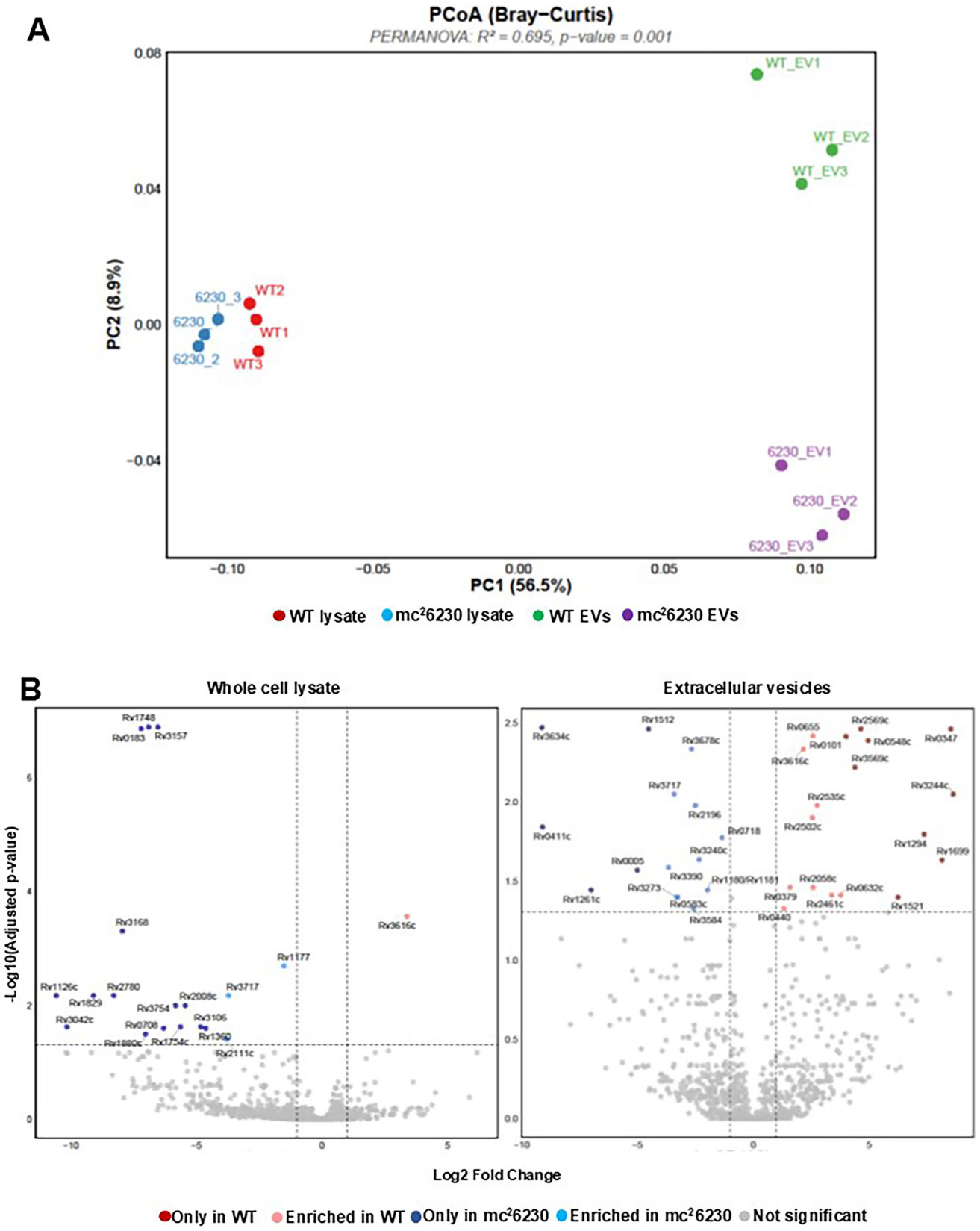

FIGURE 2 | Differential proteomics shows marginal changes in EV cargo between WT and mc^{2}6230 strains. (A) PCA plot of the proteomics data. The loadings from the two first principal components are plotted. PC1 (*X* axis) significantly separates samples across cell-compartments (One-tailed Mann Withney test: PC1 in EVs versus WC: $p = 1.08$ e-03), while PC2 mostly separates EVs samples between strains. (B) Volcano plot includes differentially expressed proteins between whole cell lysates or EVs from WT and mc^{2}6230 Mtb strains. Whole cell lysates and EVs were obtained from three independent biological MM cultures and processes by label-free mass spectrometry. Proteins were classified as not significant, enriched or unique for each strain and a color code assigned.

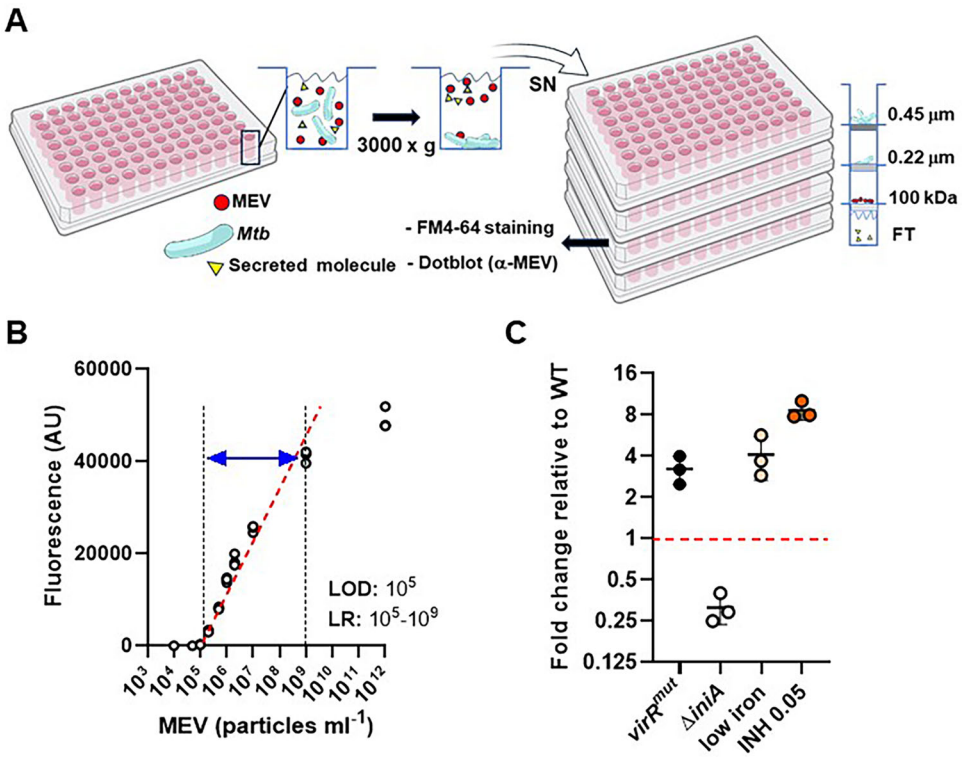

FIGURE 3 | Analytical performance of ahigh-throughput screening platform to search for genetic regulators of MEV biogenesis in Mtb. (A) Overview of the filtration-based MEV capture and quantification platform (2nd screening, 96 well). (B) Analytical performance of the platform, including limit of detection (LOD) and linearity range (LR) using purified MEVs. (C) Validation of system responsiveness using conditions that alter MEV production. Dashed line represents the WT MEV reference level adopted as 1. Data are mean and standard of error from three biological replicates. Experiments were repeated twice with similar results.

et al. 2023; Salgueiro; Bertol; and Gutierrez 2023). These results indicate that the screening system is robust enough to investigate alterations in vesiculation in *Mtb*.

Screening of the Tn mutant library. Tn mutants were initially grown in 384-well plates to stationary phase in 7H9 medium. Afterwards cultures were diluted 40-fold in 90 µL of MM without detergent. Each plate included a positive control of mc^26230 *Mtb* strain and a negative control of mc^26230 cells that had been washed; for the negative control, the washed cells were suspended in fresh MM immediately prior to processing. Mutants were grown for 7 days and processed with the screening system. To account for potential growth defects that could affect vesiculation levels, we measured optical density (OD) at the time of isolation in a parallel growth experiment using the same MM including detergent. A total of 442 mutants failed to grow under these experimental conditions and were not considered further. Supernatants were then transferred to the screening system and processed to determine MEV levels using the FM4-64 probe. This signal was normalized by optical density (Figure 4A). Using this system, we selected 136 mutants with MEV levels 2.5-fold higher or lower relative to WT, which included 77 hypervesiculating and 59 hypovesiculating mutants. To account for potential false positives and negatives, a 2nd screening was conducted in 96-well plates on the selected mutants using a MEV-specific antiserum (Prados-Rosales et al. 2014; Gupta et al. 2023) and vesiculation levels were assessed by dot blot (Figure 4B). This approach confirmed the reliability of the primary screening, retaining 117 mutants. (Figure 4C, Table S2). We then proceeded to identify the Tn insertion site in the genome of selected mutants. Previously known, the mariner Tn used for mutagenesis inserts randomly at TA dinucleotides, with most insertions occurring in ORFs (Rubin et al. 1999). Our analysis showed that most of the selected mutants harbored Tn insertion sites mapped to core gene regions. We noted that some mutants showed an increased frequency of identification in our screening, which may reflect the clonal redundancy of those mutants within the ordered library. This fact left a total of 68 genes as unique determinants of vesiculation. (Figure 5A, Table S2). We next performed an enrichment analysis by GO and found that groups of genes with a negative effect on vesiculation (mutants with hypervesiculating phenotypes) are linked to biological processes including transport of cations across the membrane, sulfur amino acid biosynthesis or suppression of host immune responses. (Figure 5B). Conversely, we found enrichment in biological processes like fatty acid biosynthesis or catabolism of carboxylic acids in the group of hypovesiculating mutants (Figure 5C). Looking at the genes more individually, we observed that mutants affected in genes involved in cell wall components synthesis pathways like peptidoglycan (PG) (*amiB2*) or tuberculostearic acid (*ufaA1*) manifested a hypervesiculating phenotype. In addition, the most frequently identified hypervesiculating mutant harbored Tn insertions in Rv1543, a predicted fatty acyl-CoA reductase involved in wax esters synthesis (Sirakova et al. 2012). Moreover, mutants in *ppe* genes like *ppe31* or *ppe62*, involved in iron or magnesium acquisition (Mitra et al. 2017; Wang et al. 2020) also showed hypervesiculation.

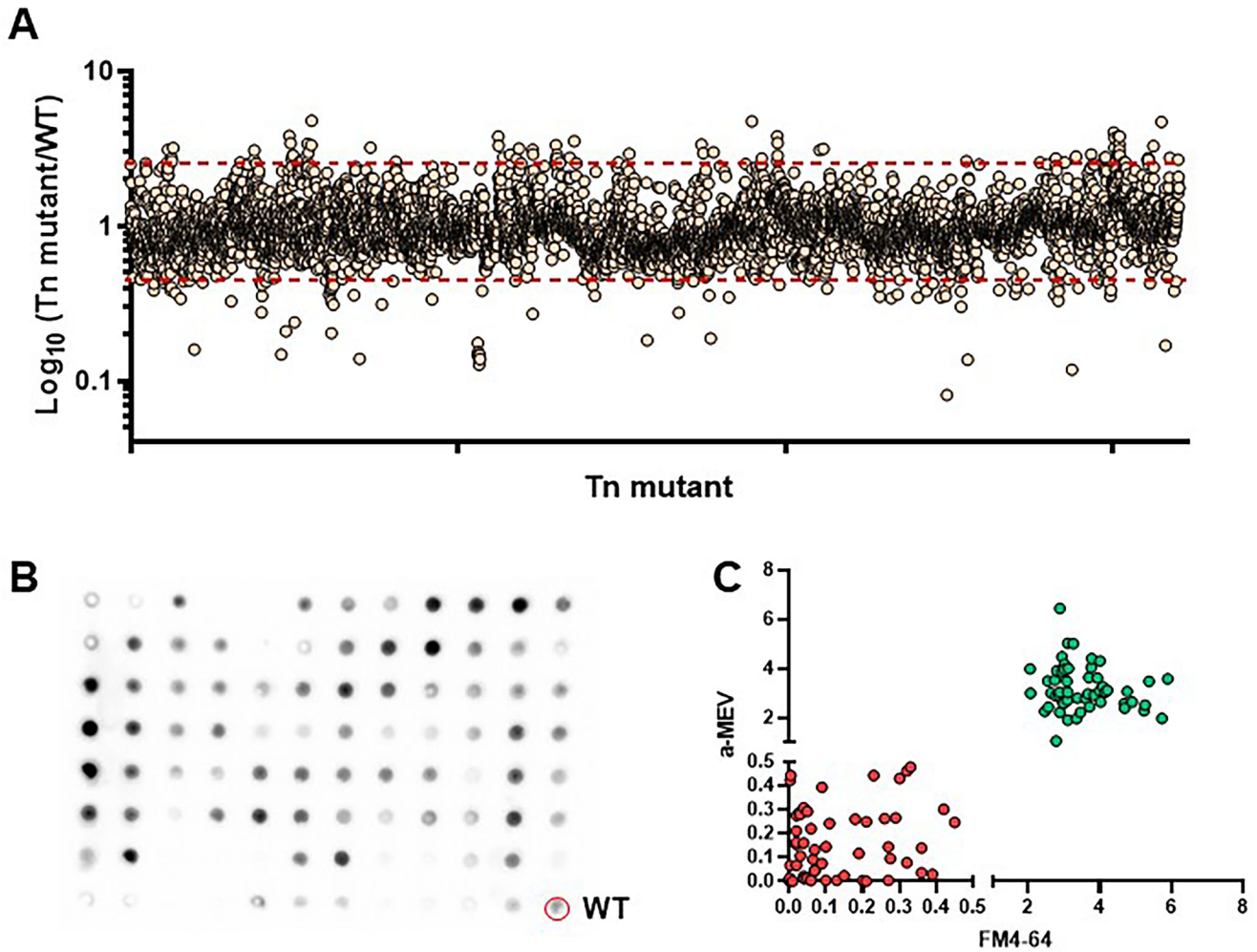

FIGURE 4 | Genome-wide screening reveals genetic determinants of vesiculation in Mtb. (A) Primary screen results from >6500 mc^{2}6230 Tn mutants. Mutants exhibiting ≥2.5-fold increases or decreases in MEV production (depicted as red dotted lines) relative to WT were submitted to secondary screening. (B) Representative 96-well plate output from 2nd screening out of two independent experiments. Similar WT levels were measured when this control was placed at a different position. (C) Correlation of MEV quantification by FM4-64 fluorescence and MEV-specific immunoblotting used in the 2nd screening. Red dots show hypovesiculating mutants and green dots show hypervesiculating mutants.

Notably, hypovesiculating mutants showed insertions in genes involved in fatty acid oxidation (*fadD* genes) or lipid degradation (*lipM*) (Figure 5A). The mutant with the highest reduction in MEV levels and higher frequency of identification corresponded to Tn:Rv0823c, with an insertion in a putative oxidoreductase upstream of a LytR-CpsA-Psr (LCP) protein (Rv0822) involved in PG remodeling and MEV release (Salgueiro, Bertol, and Gutierrez 2023). This screening identified an IniA *Tn* mutant with reduced capacity of MEV vesiculation as we have recently reported (Gupta et al. 2023). To further validate the vesiculation phenotype of some of the selected mutants, we isolated MEVs from axenic cultures and determined their concentration by NTA. Specifically, we could measure an increase in the number of particles for the hypervesiculating mutant Tn::*ufA1* relative to WT (Figure 5D) and an decrease in vesiculation levels in the hypovesicualting mutant Tn::*fadD11* relative to WT (Figure 5D).

Taking all together, this high-throughput screening system identifies that genes involved in pathways related to cations membrane transport, cell envelope remodeling including PG or mycolic acids (MA) seem to have a negative regulation on MEV production. Conversely, lipid degradation pathways are needed to promote a normal vesiculation process in *Mtb*.

3 | Discussion

Several genes and environmental determinants have been linked to MEV production. However, a genome-wide pathway-agnostic approach had not been undertaken. Our high throughput screen reveals that MEV biogenesis is complex, actively regulated process involving multiple genetic systems.

The identification of 117 genes that influence vesiculation highlights the complexity of this process and indicates that MEV production is not a passive consequence of membrane instability, but rather a controlled process. This finding is consistent with studies in *Escherichia coli* and other bacteria (McBroom et al. 2006). The co-existence of both hyper- and hypovesiculation mutants implies the existence of several regulatory nodes that can either promote or restrict MEV output. These results align with similar results in *Salmonella enterica* Serovar Typhi, where

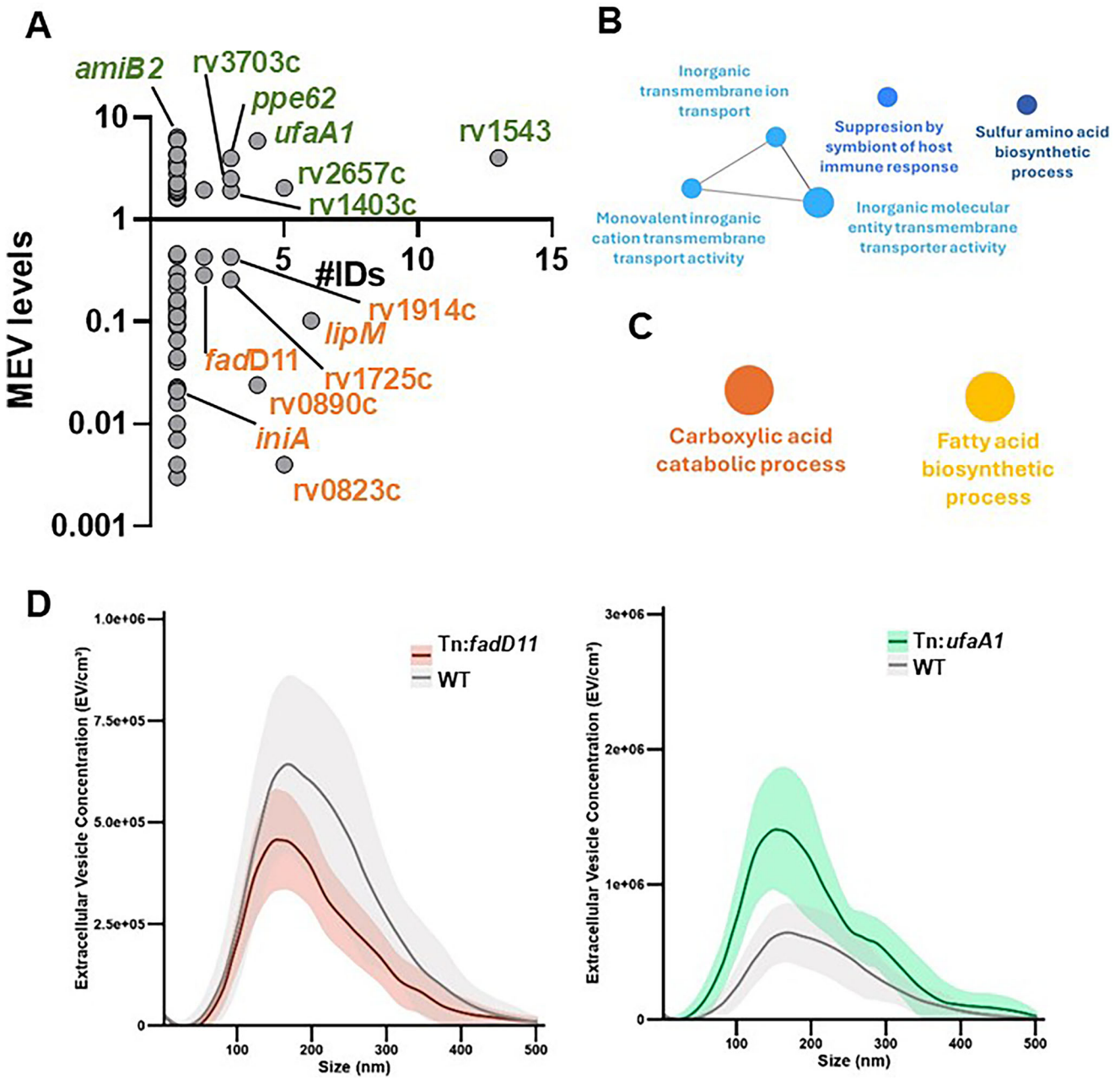

FIGURE 5 | Genes linked to cell envelope-associated biological processes and fatty acid metabolism are major genetic determinants of vesiculation in Mtb. (A) Frequency of Tn insertions of 68 validated mutants (hyper (green)- versus hypovesiculating (orange)). (B) Enriched biological processes linked to genes interrupted in hypervesiculating mutants performed by GO analysis using Clue GO. (C) Enriched biological processes linked to genes interrupted in hypovesiculating mutants performed by GO analysis using Clue GO. (D) Independent confirmation of vesiculation phenotypes for selected mutants by NTA. MEVs were isolated from three independent MM cultures and measured by NTA. Data are mean and standard of error. Experiments were repeated twice with similar results.

genes linked to capsule synthesis were found to influence outer membrane vesicles (OMV) biogenesis (Nevermann et al. 2019), reinforcing the idea that vesiculation is a conserved and tightly regulated process across bacterial species.

Despite the robustness and scalability of our high-throughput screening platform, several limitations should be considered when interpreting these findings. First, while the *mariner*-based transposon system used here provides near-random insertion across the *Mtb* genome (Rubin et al. 1999), we did not perform genetic complementation of the identified mutants within this study. Complementation experiments are being conducted as part of a separate ongoing investigation, and preliminary evidence from our laboratory confirms that the transposon insertions in most of the identified genes map to core open reading frames. Nevertheless, we cannot formally exclude the possibility that some of the observed vesiculation phenotypes arise from polar effects on adjacent genes, particularly in operonic contexts where a single insertion may disrupt the expression of downstream loci.

EV production is intrinsically linked to bacterial growth and viability, we normalized our primary screen readouts by optical density measured in parallel cultures. While this normalization effectively accounts for gross growth defects, it does not fully capture more subtle alterations in bacterial physiology—such as changes in metabolic activity, cell division rates, or stationary phase entry—that could secondarily influence vesiculogenesis. We note that the 442 mutants excluded from the screen due to frank growth failure under our experimental conditions may include strains with extreme vesiculation defects that are inseparable from their inability to proliferate. Thus, our dataset likely underestimates the full genetic landscape of MEV biogenesis by excluding essential genes or those with severe fitness costs.

The secondary screening step employed a polyclonal antiserum raised against purified MEVs from *Mtb* H37Rv. Although this reagent has been extensively validated for its specificity and sensitivity (Prados-Rosales et al. 2014), it may introduce bias towards mutants that alter the surface epitope composition of vesicles rather than their absolute quantity. For instance, a mutant that releases normal numbers of EVs but with substantially altered lipoprotein or glycolipid cargo could yield a false hypovesiculating or hypervesiculating signal in the dot-blot format. We attempted to mitigate this by cross-validating a subset of mutants (including Tn::*ufaA1* and Tn::*fadD11*) using orthogonal NTA-based quantification, which confirmed the directionality of the phenotype. However, we cannot exclude that some of the 117 retained mutants exhibit changes in vesicle immunoreactivity rather than true biogenesis defects. Future studies incorporating lipidomics or proteomics of MEVs from these mutants will help resolve this issue. Nevertheless, the fact that two different approaches to detect EVs retain most of the identified mutants suggest that EV recognition by MEV antiserum is robust enough to measure MEV levels. Indeed, we have demonstrated that immunogenicity of MEVs is restricted to six to seven antigens as measured by western blot and these antigens are conserved across different conditions that alter vesiculation in *Mtb* (Prados-Rosales et al. 2014; Schirmer et al. 2022).

Our screen recovered *iniA* as one the previously described genetic regulators of MEV production (Gupta et al. 2023), but failed to recovered *virR* or the two-component system *senX3-regX3* (White et al. 2018). The absence of *virR* from our hit list is unlikely to reflect a false negative, given that we previously characterized the mutant with a hypervesiculating phenotype. Instead, its absence in the screening is likely explained from the specific growth conditions used during the screen. *virR* expression is known to be influenced by growth phase and nutrient availability, and our use of minimal medium without detergent may not have captured the conditions under which VirR exerts its maximal regulatory effect. Similarly, the SenX3-RegX3 system responds to phosphate limitation, and our MM contains sufficient phosphate to support near-normal growth, potentially masking the vesiculation phenotype of mutants in this pathway. These observations highlight that the genetic determinants of vesiculogenesis are not static but rather context-dependent, and that screens performed under a single environmental condition will inevitably miss regulators that are conditionally active. Future iterations of this screening platform using alternative media (e.g., phosphate-limited, iron-depleted, or hypoxia-mimicking conditions) may uncover additional layers of regulation.

Finally, the use of the attenuated mc^{2}6230 (ΔRD1Δ*panCD*) strain, while necessary for BSL2 containment, may constrain the generalizability of our findings to fully virulent *Mtb*. Although our comparative proteomic analysis revealed minimal differences in whole-cell and EV protein composition between mc^{2}6230 and H37Rv, the absence of the RD1 region—which encodes the ESX-1 secretion system—could influence vesicle biogenesis or cargo sorting in ways that are not captured by steady-state proteomics. Similarly, the auxotrophy for pantothenate may subtly alter lipid metabolism, given that coenzyme A is a central cofactor in fatty acid oxidation and biosynthesis. Nevertheless, the successful validation of multiple known vesiculation phenotypes (including *iniA*, iron starvation, and antibiotic exposure) and the identification of plausible novel regulators (e.g., Rv0823c, *fadD* genes) argue that mc^{2}6230 retains core vesiculogenesis pathways relevant to pathogenic *Mtb*.

Despite these limitations, this work provides the most comprehensive genetic analysis of MEV production to date and offers a foundation for mechanistic studies. The convergence of our screen on fatty acid metabolism and cell envelope remodeling echoes findings in Gram-negative systems, suggesting evolutionarily conserved principles of bacterial vesicle biogenesis. Future work incorporating complementation, conditional alleles, and orthogonal detection methods will be essential to validate the 68 genetic determinants identified here and to dissect their molecular roles. Improved understanding of vesiculogenesis may enable new approaches for TB diagnostics, vaccines, and host–pathogen interaction research.

4 | Materials and Methods

Bacteria and culture. *Mtb* H37Rv (ATCC) was initially grown in Middlebrook 7H9 medium (7H9) supplemented with 10% (v/v) OADC enrichment (Becton Dickinson Microbiology Systems, Spark, MD), 0.5% (v/v) glycerol and with or without Tyloxapol 0.05% (v/v; Sigma). Alternatively, *Mtb* was also grown in a minimal medium (MM) before MEV isolation consisting of KH_2PO_4 1 g/l, Na_2HPO_4 2.5 g/l, asparagine 0.5 g/l, ferric ammonium citrate 50 mg/l, $CaCl_2$ 0.5 mg/l, $ZnSO_4$ 0.1 mg/l, with or without Tyloxapol 0.05% (v/v), containing 0.1% (v/v) glycerol, pH 7.0. *Mtb* ΔRD1Δ*panCD* (mc^{2}6230) double auxotroph strain (gifted from Dr. William R. Jacobs, Jr., Albert Einstein College of Medicine, NY, USA) was grown as above but supplemented with 0.024 mg/ml calcium pantothenate (Sigma-Aldrich). *Mtb* mc^{2}6230 cultures were subjected to iron starvation or treated with Isoniazid following published protocols (Gupta et al. 2023).

Construction of the transposon (Tn) mutant library. *Mtb* mc^{2}6230 was used as a parental strain for construction of the Tn mutant library. Mycobacterial phage phAE180 (Kriakov et al. 2003) (gifted from Dr. William R. Jacobs, Jr., Albert Einstein College of Medicine, NY, USA) was used for transducing transposon into the *Mtb* mc^{2}6230 bacterial cells. The backbone of phAE180 is a temperature-sensitive bacteriophage TM4 and phAE180 has a mariner-class transposon element (Himar1) identified from horn flies *Haematobia irritans* (Lampe et al. 1999). *Mtb* mc^{2}6230 mariner-based transposon mutagenesis was carried out as previously described (Kriakov et al. 2003). *Mtb* mc^{2}6230 was inoculated in Middlebrook 7H9 medium containing 0.2% glycerol, 0.1%

Tween 80 (MP Biomedicals, Illkirch, France) and 10% Middlebrook albumin-dextrose-catalase (OADC) (7H9/OADC/Tween 80), 0.024 mg/ml calcium pantothenate (Sigma-Aldrich), supplemented with 40 μg/ml kanamycin. One hundred milliliter of broth cultures were grown to optical densities around 1.0. After harvesting the bacteria by centrifugation, 10 ml of high titer MycoMarT7 phagemids ($>1\times10^9$ PFU/ml) suspended in MP buffer (50 mM Tris-HCl [pH 7.5], 150 mM NaCl, 2 mM $CaCl_2$) was transduced at 37 °C overnight. After centrifugation, the harvested bacteria were resuspended in 10 ml of 7H9/OADC/Tween 80, inoculated on Middlebrook 7H10 solid medium supplemented with 10% OADC (Becton Dickinson and Co., Sparks, MD) (7H10/OADC) agar plates containing 30 μg/ml kanamycin, and cultured at 37 °C for 2 weeks. The kanamycin-resistant colonies ($>1\times10^5$) were evenly resuspended in 7H9/OADC containing 20% glycerol, aliquoted and stored at −80 °C until further use. Approximately 6500 single colonies were manually picked and transferred to individual wells in 384-well plates containing Middlebrook 7H9 medium containing 0.2% glycerol, 0.1% Tween 80, 10% Middlebrook OADC (7H9/OADC/Tween 80), 0.024 mg/ml calcium pantothenate (Sigma-Aldrich), supplemented with 30 μg/ml kanamycin (7H9/OADC/T80/CP/KAN), grown to stationary phase for downstream screening or stored at −80°C including 10% glycerol.

Tn mutant screening. The Tn mutants were initially grown in 384-well plates to stationary phase in 7H9/OADC/T80/CP/KAN. Afterwards, cultures were diluted 40-fold in 90 μL of MM supplemented with 0.024 mg/ml calcium pantothenate (Sigma-Aldrich), and 30 μg/ml kanamycin but without OADC nor detergent. Each plate included a positive control of *Mtb* $mc^2$6230 cells and a negative control of MM alone. Cells were grown for 7 days prior to being centrifuged at 1500 rpm for 15 min at 4°C. Supernatants were transferred to a 384-well plate equipped with a 0.45 μm membrane at the bottom, which in turn was mounted on top of another 384-well plate equipped with a 0.2 μm membrane at the bottom. The 0.2 μm membrane is needed to make sure that no bacteria are retained with the MEV fraction. Both plates were supported by another 384-well plate equipped with a 100-kDa membrane. The three plates were laid on a standard 384-well plate, which retained the flow-through after centrifugation at 3000 rpm for 25 min. As in the standard protocol for MEV isolation (Prados-Rosales et al. 2011; Prados-Rosales et al. 2014), MEVs are retained at the 100-kDa membrane. Further, this retentate was reconstituted in 15 μL of PBS. In the 1st screening 5 μL of the supernatant was incubated with FM4-64 (Molecular Probes) (3.3 μg/ml in phosphate-buffered saline for 10 min at 37°C). Vesicles alone and FM4-64 probe alone were positive and negative controls. After excitation at 506 nm, the emission at 750 nm was measured with a Molecular Devices SpectraMAX GeminiXS fluorometer. In the secondary screening the retained MEVs were transferred to a vacuum manifold system with a 0.45 μm high-protein binding nitrocellulose membrane. The nitrocellulose membrane was immunoblotted using mouse antiserum recognizing MEVs (Prados-Rosales et al. 2014). Antigen-antibody complexes were detected using anti mouse IgG and the ECL prime Western Blotting Detection chemiluminescent kit (GE Healthcare). The signal was visualized in a Chemidoc MP imaging system (BIO-RAD). Spot intensities were analyzed by densitometry using ImageJ (Schneider, Rasband, and Eliceiri 2012). Backgrounds were determined for each dot individually and set as a straight line at the lowest point of the histological profile of the lane. This vacuum-assisted dot blot system does not suffer from corner effects as all aspirated supernatants are submitted to the same aspiration force and after several min working under vacuum no liquid is left, indicating that all samples go through the nitrocellulose membrane. Examination of WT levels at different positions across the membrane confirmed this.

To account for potential growth defects of mutants, we ran a parallel experiment including MM with detergent to determine optical density at 600 nm (OD^{600nm}). MEV production for each mutant was calculated by dividing immunoblot or the FM4-64 signals by OD^{600nm}. The relative MEV production was further calculated by dividing MEV production of the mutants by that of the parental strain in each experiment.

Mapping Tn insertion site. Chromosomal DNA was extracted from selected Tn mutants and digested with BssHII prior to ligation and transformation of *E. coli* DH5$\alpha\lambda$pir. Plasmid DNA of kanamycin resistant transformants was sequenced with upstream and downstream primers m4R1 (5´TAGACCGAGATAGGGTTGAG3´) and m4F1 (5´GCATCGCCTTCTATCGCCTTC3´), respectively. Transposon-chromosome junctions were identified by comparing relevant plasmid-derived sequences with the *Mtb* H37Rv genome sequence using the NCBI genome BLAST.

Isolation of MEVs. MEVs were prepared and purified as previously described (Prados-Rosales et al. 2011). Briefly, the culture filtrate of 1 L cultures of *Mtb* grown in MM supplemented with calcium pantothenate and without detergent for 14 days was processed for vesicle isolation by differential centrifugation. In parallel, a 2 mL culture in similar medium supplemented with 0.05% tyloxapol to disperse bacterial clumps were used to determine viability by plating culture dilutions onto 7H10 agar plates and enumerating colony-forming unit (CFU) at the time of culture filtrate collection. The membranous pellet containing vesicles, protein aggregates and capsule polysaccharides obtained after ultracentrifugation of the culture filtrate at 100,000 ×g for 2 h at 4°C, was resuspended in 1 mL sterile PBS and overlaid with a series of Optiprep gradient layers with concentrations ranging from 45% to 20% (w/v). The gradients were centrifuged at 100,000 × g for 16 h. At the end 1 mL fractions were removed from the top, diluted to 20 mL with PBS and purified vesicles recovered by sedimentation at 100,000 × g for 1 h. Vesicle pellets were suspended in PBS before analysis.

Label-free mass spectrometry analysis. Whole cell lysates (WCL) were obtained from 5 mg of cell biomass of *Mtb* MM cultures (3 biological replicates). *Mtb* cells were first transferred to a low-binding protein microtube and washed with 1 mL of PBS to remove exogenous proteins. Next, they were centrifuged for 2 min at 10,000 x g and the PBS buffer was removed. The pellet was suspended in 500 μL of lysis buffer (PBS supplemented with protein inhibitor cocktail (Roche)) and transferred to a bead-beating tube including 0.5 mm glass beads. Bacteria were lysed 5 times with 20 s cycles of Fast Prep bead beater (MP Biochemicals) at a speed of 6.0 m/s with 1 min rest on ice between each cycle. Cell lysate was centrifuged for 5 min at 10,000 x g and the supernatant was recovered as WCL in a new tube. Isolated bacterial EVs

were directly processed for proteomics with no prior lysis. WCL and EV proteins from WT and mc^{2}6230 *Mtb* were analyzed by label-free LC-MS using a Synapt G2Si ESI Q-Mobility-TOF mass spectrometer (Waters) coupled online to a NanoAcquity nano-HPLC system (Waters). Chromatographic separation was performed on a Waters BEH C18 nano-column (200 mm x 75 um inner diameter, 1.8 um). Protein samples were processed and digested according to the filter-aided sample preparation (FASP) protocol (Wiśniewski et al., 2009). Trypsin was added at a 1:50 trypsin-to-protein ratio and digestion proceeded overnight at 37°C. Peptide mixtures were then dried in an RVC2 25 SpeedVac concentrator (Christ) and reconstituted in 0.1% FA. Prior to LC-MS analysis, peptides were desalted using C18 StageTips (Millipore) and finally resuspended in 0.1% FA.

A total of 500 ng of digested peptides were injected into the LC system and separated over a 60 min elution gradient ranging from 5% to 60% ACN. Data acquisition was performed in HDDA mode, which improves signal detection through an ion mobility separation step. Protein identification and quantification were conducted using Progenesis LC-MS software (version 2.0.5556.29015, Nonlinear Dynamics). One LC-MS run was designated as the reference for aligning precursor masses across all samples. Only peptide features with charge states of 2+ or 3+ were considered for downstream analysis.

Raw feature abundances were automatically normalized and log-transformed relative to the selected reference run. Samples were then organized according to the comparison of interest, and statistical significance was assessed using ANOVA. A comprehensive peak list containing all detected features was generated and exported to the Mascot search engine (Matrix Science Ltd.). Database searching was performed against the UniProt/SwissProt protein repository, and the resulting list of identified peptides was subsequently re-imported into Progenesis LC-MS. Protein quantification was carried out using the three most intense non-conflicting peptides (i.e., peptides uniquely assigned to a single protein), except for proteins with only two non-conflicting peptides.

Proteomics data analysis. Normalization and imputation of the proteomics intensity data was carried out using the DEP package in R (Zhang et al. 2018). For normalization, the vsn approach (Huber et al. 2002) was applied, which stabilizes the variance and corrects for heteroscedasticity across the dataset. Missing values were imputed using the bpca method (Oba et al. 2003), which imputes the missing values leaning on principal component analysis. Proteins were considered strain-specific when detected in at least two replicates of one strain and not detected in the other.

Differential protein abundance analysis was conducted using limma package in R (Ritchie et al. 2015). To control multiple testing, *p*-values were adjusted using the Benjamini-Hochberg procedure (False Discovery Rate, FDR). Proteins with an adjusted *p*-value < 0.05 and an absolute log2 fold-change greater than 1 were considered significantly enriched. For classification as condition-specific, unique to a given sample, a stricter threshold of an absolute log2 fold-change greater than 4 was applied.

To evaluate global differences in protein abundance profiles, Principal Coordinate Analysis (PCoA) based on Bray-Curtis dissimilarities was performed using the vegan R package (Oksanen et al. 2025). Statistical significance of the separation between experimental conditions was assessed via PERMANOVA using the adonis2 function. Additionally, volcano plots generated with ggplot2 and ggrepel illustrated the relationship between fold-change magnitude and statistical significance, highlighting the most relevant differentially expressed proteins along with their specific Rv numbers.

Gene ontology (GO) enrichments. All the enrichment analyses of the differentially expressed proteins were performed with the ClueGO v2.5.10 plugin within Cytoscape 3.10.4 (Bindea et al. 2009). As input for the ClueGO analyses genes were used, after mapping the protein identifiers obtained from LC-MS quantification using UniProtKB. *Mycobacterium tuberculosis* genome was downloaded and loaded into ClueGO. Biological process, molecular function and cellular component analyses were performed according to a two-sided right-sided hypergeometric test. The resulting *p*-values were corrected for multiple testing using the Benjamini-Hochberg false discovery rate (FDR) procedure and GO terms with FDR < 0.05 were considered significantly enriched. Functional grouping was controlled using a Kappa score threshold of 0.4. Additional filtering criteria were applied to ensure biological specificity and robustness: each GO term was required to represent at least 3%–5% of the genes within the submitted dataset and only GO terms spanning levels 3–8 of the ontology hierarchy were included to avoid categories that were either too broad or overly specific.

Nanoparticle tracking analysis (NTA). NTA was conducted using ZetaView (Particle Metrix). Instrument calibration was performed prior to EV analysis using 102 nm polystyrene beads (Thermo Fisher Scientific, USA), according to manufacturer instructions. Measurements were performed using a 405 nm 68 mW laser and CMOS camera by scanning 11 cell positions and capturing 60 frames per position at 25 C with camera sensitivity 85, shutter speed 100, autofocus and automatic scattering intensity. Samples were diluted in pre-filtered PBS to approximately 10^6–10^7 particles·ml-1 in Millipore DI water. Analysis was performed using ZetaView Software version 8.05.12 SP1 with a minimum brightness of 30, maximum brightness of 255, minimum area of 5, maximum area of 1000, and s minimum trace length 15. Triplicate videos of each sample were taken in light scatter mode. Particle size and concentration were analyzed using the built-in EMV protocol and plotted using graph pad prism 8.0 software.

Statistics. Data representation and statistical analyses were performed using GraphPad Prism version 9.0 or R-studio. Data are presented as mean ± standard error of at least three independent biological replicates. Following a significant two-way, Tukey's significant difference test was applied for all pairwise comparisons. A *p*-value of less than 0.05 was considered statistically significant. In figures, asterisks denote significance levels (*$p < 0.05$, **$p < 0.01$, ***$p < 0.001$, ****$p < 0.0001$) derived from the Tukey's post-hoc test results.

Author Contributions

José L. Serrano-mestre, **Laura Lerma**, **Lucía Vázquez-iniesta**, **Vivian C. Salgueiro-toledo**, **Ainhoa Palacios**, **Andrea Doddi**, **Sogol Alebouyeh**, **Felix Elortza**, **Mikel Azkargorta**, **Leticia Sampedro, Estibaliz Atondo** and **Miguel Ángel Pacual-itoiz** performed research and analyzed data; **Torin Westwood** generated reagents; **William R. Jacobs Jr** designed the study and wrote the paper; **Rafael Prados-rosales** designed the study, wrote the paper and managed the submission.

Acknowledgements

R.P.-R. acknowledges support by MINECO/FEDER EU contracts SAF2016–77433-R, PID2019-110240RB-I00, PID2022-136611OB-I00; and NIH-R01AI162821. CICbioGUNE thanks MINECO for the Severo Ochoa Excellence Accreditation (SEV-2016–0644).

Conflicts of Interest

The authors declare no competing interests.

Data Availability Statement

The data that support the findings of this study are available from the corresponding author upon reasonable request.

References

Abdallah, A. M., N. C. Gey van Pittius, P. A. DiGiuseppe Champion, et al. 2007. "Type VII Secretion—Mycobacteria Show the Way." *Nature Reviews Microbiology* 5, no. 11: 883–891.

Athman, J. J., Y. Wang, D. J. McDonald, W. H. Boom, C. V. Harding, and P. A. Wearsch. 2015. "Bacterial Membrane Vesicles Mediate the Release of Mycobacterium Tuberculosis Lipoglycans and Lipoproteins from Infected Macrophages." *Journal of Immunology* 195, no. 3: 1044–1053. https://www.ncbi.nlm.nih.gov/pubmed/26109643.

Bindea, G., B. Mlecnik, H. Hackl, et al. 2009. "ClueGO: a Cytoscape Plug-in to Decipher Functionally Grouped Gene Ontology and Pathway Annotation Networks." *Bioinformatics* 25, no. 8: 1091–1093.

Bishop, D. G., and E. Work. 1965. "An Extracellular Glycolipid Produced by Escherichia Coli Grown Under Lysine-Limiting Conditions." *Biochemical Journal* 96, no. 2: 567–576. https://www.ncbi.nlm.nih.gov/pubmed/4953781.

Brown, L., J. M. Wolf, R. Prados-Rosales, and A. Casadevall. 2015. "Through the Wall: Extracellular Vesicles in Gram-Positive Bacteria, Mycobacteria and Fungi." *Nature Reviews Microbiology* 13, no. 10: 620–630. https://www.ncbi.nlm.nih.gov/pubmed/26324094.

Daffé, M. 2015. "The Cell Envelope of Tubercle bacilli." *Tuberculosis* 95, no. S1: S155–S158. https://www.ncbi.nlm.nih.gov/pubmed/25819158.

Dulberger, C. L., E. J. Rubin, and C. C. Boutte. 2019. "The Mycobacterial Cell Envelope—A Moving Target." *Nature Reviews Microbiology* 18, no. 1: 47–59. https://www.ncbi.nlm.nih.gov/pubmed/31728063.

Gupta, S., M. Bhagavathula, V. Sharma, et al. 2023. "Dynamin-Like Proteins Mediate Extracellular Vesicle Secretion in Mycobacterium Tuberculosis." *EMBO Reports* 24, no. 6: e55593.

Huber, W., A. von Heydebreck, H. Sültmann, A. Poustka, and M. Vingron. 2002. "Variance Stabilization Applied to Microarray Data Calibration and to the Quantification of Differential Expression." *Bioinformatics* 18: S96–S104. http://www.dkfz.de/abt0840/whuber.

Kalscheuer, R., A. Palacios, I. Anso, et al. 2019. "The Mycobacterium Tuberculosis Capsule: A Cell Structure With key Implications in Pathogenesis." *Biochemical Journal* 476, no. 14: 1995–2016. https://www.ncbi.nlm.nih.gov/pubmed/31320388.

Kriakov, J., S. H. Lee, and W. R. Jacobs. 2003. "Identification of a Regulated Alkaline Phosphatase, a Cell Surface-Associated Lipoprotein, in Mycobacterium Smegmatis." *Journal of Bacteriology* 185, no. 16: 4983–4991.

Lampe, D. J., B. J. Akerley, E. J. Rubin, J. J. Mekalanos, and H. M. Robertson. 1999. "Hyperactive Transposase Mutants of the Himar1 Mariner Transposon." *Proceedings of the National Academy of Sciences* 96, no. 20: 11428–11433.

McBroom, A. J., A. P. Johnson, S. Vemulapalli, and M. J. Kuehn. 2006. "Outer Membrane Vesicle Production by Escherichia Coli is Independent of Membrane Instability." *Journal of Bacteriology* 188, no. 15: 5385–5392.

Mitra, A., A. Speer, K. Lin, S. Ehrt, and M. Niederweis. 2017. "PPE Surface Proteins are Required for Heme Utilization by Mycobacterium Tuberculosis." *American Society for Microbiology* 8, no. 1: e01720-16.

Nagakubo, T., Y. O. Tahara, M. Miyata, N. Nomura, and M. Toyofuku. 2021. "Mycolic Acid-Containing Bacteria Trigger Distinct Types of Membrane Vesicles Through Different Routes." *iScience* 24, no. 1: 102015.

Nevermann, J., A. Silva, C. Otero, et al. 2019. "Identification of Genes Involved in Biogenesis of Outer Membrane Vesicles (OMVs) in Salmonella Enterica Serovar Typhi." *Frontiers in Microbiology* 10: 104.

Oba, S., M. A. Sato, I. Takemasa, M. Monden, K. I. Matsubara, and S. Ishii. 2003. "A Bayesian Missing Value Estimation Method for Gene Expression Profile Data." *Bioinformatics* 19, no. 16: 2088–2096.

Oksanen, J. G. L. Simpson, F. Guillaume Blanchet, et al. Community Ecology Package [Package "vegan"]. CRAN. 2025.

Prados-Rosales, R., A. Baena, L. R. Martinez, et al. 2011. "Mycobacteria Release Active Membrane Vesicles That Modulate Immune Responses in a TLR2-dependent Manner in Mice." *Journal of Clinical Investigation* 121, no. 4: 1471–1483. https://www.ncbi.nlm.nih.gov/pubmed/21364279.

Prados-Rosales, R., L. Brown, A. Casadevall, S. Montalvo-Quirós, and J. L. Luque-Garcia. 2014. "Isolation and Identification of Membrane Vesicle-Associated Proteins in Gram-Positive Bacteria and Mycobacteria." *MethodsX* 1: 124–129. https://www.ncbi.nlm.nih.gov/pubmed/26150943.

Prados-Rosales, R., L. J. Carreño, A. Batista-Gonzalez, et al. 2014. "Mycobacterial Membrane Vesicles Administered Systemically in Mice Induce a Protective Immune Response to Surface Compartments of Mycobacterium Tuberculosis." *mBio* 5, no. 5: e01921-14.

Prados-Rosales, R., B. C. Weinrick, D. G. Piqué, et al. 2014. "Role for Mycobacterium Tuberculosis Membrane Vesicles in Iron Acquisition." *Journal of Bacteriology* 196, no. 6: 1250–1256. https://www.ncbi.nlm.nih.gov/pubmed/24415729.

Rath, P., C. Huang, T. Wang, et al. 2013. "Genetic Regulation of Vesiculogenesis and Immunomodulation in Mycobacterium Tuberculosis." *Proceedings of the National Academy of Sciences* 110, no. 49: E4790–E4797. https://www.ncbi.nlm.nih.gov/pubmed/24248369.

Ritchie, M. E., B. Phipson, D. Wu, et al. 2015. "Limma Powers Differential Expression Analyses for RNA-Sequencing and Microarray Studies." *Nucleic Acids Research* 43, no. 7: e47.

Rubin, E. J., B. J. Akerley, V. N. Novik, D. J. Lampe, R. N. Husson, and J. J. Mekalanos. 1999. "In Vivo Transposition of Mariner-Based Elements in Enteric Bacteria and Mycobacteria." *Proceedings of the National Academy of Sciences* 96, no. 4: 1645–1650.

Salgueiro, V., J. Bertol, C. Gutierrez, et al. 2023. "Maintenance of Cell Wall Remodeling and Vesicle Production are Connected in Mycobacterium Tuberculosis." *eLife* 00. https://doi.org/10.7554/eLife.94982.

Sambandamurthy, V. K., S. C. Derrick, T. Hsu, et al. 2006. "Mycobacterium Tuberculosis ΔRD1 ΔpanCD: A Safe and Limited Replicating Mutant Strain That Protects Immunocompetent and Immunocompromised Mice Against Experimental Tuberculosis." *Vaccine* 24, no. 37–39: 6309–6320.

Schirmer, S., L. Rauh, S. Alebouyeh, et al. 2022. "Immunogenicity of Mycobacterial Extracellular Vesicles Isolated From Host-Related Conditions Informs About Tuberculosis Disease Status." *Frontiers in Microbiology* 13: 907296.

Schneider, C. A., W. S. Rasband, and K. W. Eliceiri. 2012. "NIH Image to ImageJ: 25 Years of Image Analysis." *Nature Methods* 9: 671–675.

Schwechheimer, C., and M. J. Kuehn. 2015. "Outer-Membrane Vesicles From Gram-Negative Bacteria: Biogenesis and Functions." *Nature Reviews Microbiology* 13, no. 10: 605–619. https://www.ncbi.nlm.nih.gov/pubmed/26373371.

Sirakova, T. D., C. Deb, J. Daniel, et al. 2012. "Wax Ester Synthesis Is Required for Mycobacterium Tuberculosis to Enter in Vitro Dormancy." *PLoS One* 7, no. 12: e51641.

Toyofuku, M., N. Nomura, and L. Eberl. 2019. "Types and Origins of Bacterial Membrane Vesicles." *Nature Reviews Microbiology* 17, no. 1: 13–24. https://www.ncbi.nlm.nih.gov/pubmed/30397270.

Wang, Q., H. I. M. Boshoff, J. R. Harrison, et al. 2020. "PE/PPE Proteins Mediate Nutrient Transport Across the Outer Membrane of Mycobacterium Tuberculosis." *Science* 367, no. 6482: 1147–1151.

Wang, X., C. D. Thompson, C. Weidenmaier, and J. C. Lee. 2018. "Release of Staphylococcus Aureus Extracellular Vesicles and Their Application as a Vaccine Platform." *Nature Communications* 9, no. 1: 1379. https://www.ncbi.nlm.nih.gov/pubmed/29643357.

White, D. W., S. R. Elliott, E. Odean, L. T. Bemis, and A. D. Tischler. 2018. "Mycobacterium Tuberculosis Pst/SenX3-RegX3 Regulates Membrane Vesicle Production Independently of ESX-5 Activity." *mBio* 9, no. 3: e00778–18. https://www.ncbi.nlm.nih.gov/pubmed/29895636.

Zhang, X., A. H. Smits, G. B. van Tilburg, H. Ovaa, W. Huber, and M. Vermeulen. 2018. "Proteome-Wide Identification of Ubiquitin Interactions Using UbIA-MS." *Nature Protocols* 13, no. 3: 530–550.

Ziegenbalg, A., R. Prados-Rosales, E. R. Jenny-Avital, R. S. Kim, A. Casadevall, and J. M. Achkar. 2013. "Immunogenicity of Mycobacterial Vesicles in Humans: Identification of a new Tuberculosis Antibody Biomarker." *Tuberculosis* 93, no. 4: 448–455. https://www.ncbi.nlm.nih.gov/pubmed/23562367.

Supporting Information

Additional supporting information can be found online in the Supporting Information section.

Supporting Information: Table 1. Proteomics analysis of whole cell lysates and EVs between WT and mc26230 Mtb. **Supporting Information**: Table 2. Quantitative vesiculation levels of the selected Tn mutants by 1st and 2nd screening.